Protein Nanoparticle Osmotic Pressure Modifies Nonselective Permeability of the Blood Brain Barrier by Increasing Membrane Fluidity

Chen Li
Nanjing University of Chinese Medicine
LinLin Chen
Nanjing University of Chinese Medicine
YuanYuan Wang
Nanjing University of Chinese Medicine
TingTing Wang
Nanjing University of Chinese Medicine
Dong Di
Nanjing University of Chinese Medicine
Hao Zhang
Nanjing University of Chinese Medicine
HuanHuan Zhao
Nanjing University of Chinese Medicine
Xu Shen
Nanjing University of Chinese Medicine
Jun Guo (guoj@njucm.edu.cn)
Nanjing University of Chinese Medicine

Research

Keywords: Blood brain barrier, Protein nanoparticle osmotic pressure, Occludin/ZO1 tension, Permeability, Membrane fluidity

Posted Date: November 4th, 2020

DOI: https://doi.org/10.21203/rs.3.rs-100354/v1

Abstract

Background

Intracellular tension plays a crucial role in the destruction of the blood brain barrier (BBB) in response to lesion stimuli. Tight junction structure could be primarily affected by tension activity. In this study, we aimed to determine the effects of extracellular BBB damage on intracellular tension activity, and elucidate the mechanism underlying the effects of intracellular protein nanoparticle-dependent osmotic pressure on BBB permeability.

Methods

The intracellular tension for tight junction proteins occludin and ZO1 were evaluated using the fluorescence resonance energy transfer (FRET)-based tension probes and cpstFRET analysis. The efficiency of the probes was examined by acceptor photobleaching FRET (FRET-AB) analysis. The changes in mobility ratios of the transmembrane protein occludin were evaluated via the fluorescence recovery after photobleaching (FRAP) test. The cytoplasmic osmotic pressure (OP) was measured using the Osmomat 3000 Freezing Point Osmometer and 050 Membrane Osmometer. The count rate of cytoplasmic nanoparticles was detected by Nanosight NS300. The activation of cofilin and stathmin was examined by Western blot analysis. The BBB permeability *in vivo* was determined via investigating the changes of Evans Blue (EB) injected into the SD rats. The tight junction formation was assessed by the measurement of transendothelial electrical resistance (TEER). Intracellular calcium or chloride ions were measured using Fluo-4 AM or MQAE dyes.

Results

BBB lesions were accompanied by changes in occludin/ZO1 tension. Increases in intracellular osmotic pressure were involved in alteration of BBB permeability, possibly through the depolymerization of microfilaments or microtubules and mass production of protein nanoparticles according to the Donnan effect. Recovery of protein nanoparticle osmotic pressure could effectively reverse the effects of changes in occludin/ZO1 tension and BBB lesions. Outward tension of intracellular osmotic potential also caused upregulation of membrane fluidity, which promoted nonselective drug influx.

Conclusions

Our results suggest a crucial mechanical mechanism underlying BBB lesions, and protein nanoparticle osmotic pressure could be a novel therapeutic target for BBB lesion-related brain diseases. Our results also provide a basis for further studies on the regulation of intracellular tension activity and its effect on the permeability of the BBB, and development of novel drugs that cross the blood-brain barrier.

Background

The blood-brain barrier (BBB) is the physical interface that separates neural tissue from peripheral blood, and is a pluricellular vascular structure formed by capillary endothelial cells[1]. The BBB plays a vital role in blocking nonselective substances such as ions, neurotransmitters, macromolecules, and neurotoxins, and in brain nutrition influx and efflux[2]. Alteration of the BBB physical structure depends on intracellular tension activity, which plays a crucial role in regulation of nonselective BBB permeability and dysfunction[3, 4]. The mechanical mechanism underlying the role of endothelial cells in BBB lesions and related therapeutic measures are of great clinical interest.

The low passive permeability of the BBB depends on sealing tight junctions formed by the junctional complexes (tight, adherens, and gap junctions) between brain endothelial cells[5]. Tight junction (TJ) proteins, including claudins and occludin, can form intermembrane bindings through homo- and heterogenous interactions between the adjacent cells, and block chemical influx and efflux through the BBB[6, 7]. The TJ plaque proteins on the cytoplasmic side are linked to the actin cytoskeleton and provide pivotal physical support for the barrier. The interaction between occludin and TJ scaffolding proteins such as ZO-1 and ZO-2, and the cytoskeletal protein F-actin are essential for the construction and stability of TJ protein complexes [8–11]. Modulation of transmembrane junctional protein complexes and poor permeability of the BBB are closely related to intracellular cytoskeletal tension.

Intracellular tension depends on cytoskeletal structure, and is mainly caused by microfilament (MF) and microtubule (MT) forces and osmotic pressure (OP)[12, 13]. Under the effect of dynamic molecules, MF and MT can produce cytoskeletal forces. The osmotic pressure (OP) difference across the membrane can produce tension by pulling the intermediate filament (IF)[10, 14]. However, the mechanisms by which cytoskeletal forces and osmotic pressure regulate the mobility of transmembrane proteins and permeability of the BBB remain unclear. Changes in extracellular osmolality can regulate BBB permeability by “pulling” the cytoskeleton [12]. We speculated that the tension of occludin/ZO-1 proteins is regulated by MF or MT forces and osmotic pressure, which could be closely related to the regulation of permeability in brain microvascular endothelial cells.

Depolymerization of MF and MT cytoskeletons could increase intracellular protein nanoparticle-dependent osmotic pressure[13, 15]. Changes in osmotic pressure across the membrane are accompanied by a change in membrane fluidity[16, 17]. The high flow of the membrane likely promotes membrane permeability, which is manifested by the fluidity of lipids and transmembrane proteins. The fluidity of membrane proteins could also be regulated by a cytoskeletal “pull”, which maintains and stabilizes the connection between transmembrane proteins and intracellular IF. However, the role of intracellular cytoskeletal tension and osmotic pressure in the regulation of membrane fluidity and permeability remains unclear.

In this study, we constructed tension probes based on fluorescence resonance energy transfer (FRET) to study the vector pull of occludin and ZO-1 tension and OP [18, 19], and determined the effects of extracellular causes of BBB damage on intracellular tension activity. We also studied the mechanical

mechanism underlying the effects of intracellular protein nanoparticle-dependent osmotic pressure on BBB permeability, and the involvement of lipid membrane fluidity and transmembrane proteins mobility.

Methods

Cell culture

The human brain microvascular endothelial cell (HBMEC) line was acquired from the BeNa Culture Collection (BNCC, Suzhou, China) and authenticated by the Genetic Testing Biotechnology Corporation (Suzhou, China) by using short tandem repeats (STR). Mycoplasma Plus PCR Primer Set (Agilent, Santa Clara, USA) was used to test for mycoplasma contamination, and results were negative. HBMEC cells were cultured in Dulbecco's Modified Eagle's Medium (Gibco, New York, USA) containing 10% fetal bovine serum (Gibco, New York, USA), 100 units/mL penicillin, and 100 μg/mL streptomycin (Gibco) and maintained in a 5% CO_2 incubator at 37°C.

Antibodies and Reagents

Phospho-cofilin and Phospho-stathmin-1 antibodies were purchased from Cell Signaling Technology (Danvers, MA, USA). Cofilin and Stathmin antibodies were purchased form proteintech (Chicago, USA). β-actin and α-tubulin antibodies were from Boster (Wuhan, China). HRP-labeled anti-rabbit and anti-mouse antibodies were purchased from Zsgb-Bio (Beijing, China).

Cytochalasin D and nocodazole were purchased from Sigma-Aldrich (Saint Louis, MO, USA). Glutamate, hydrogen peroxide, jasplakinolide, and taxol were purchased from Sigma-Aldrich (Saint Louis, MO, USA). Human vascular endothelial growth factor (VEGF) and histamine were obtained from Peprotech (Rocky Hill, NJ, USA). LPS, TNF-α, Ang-□, and Capsaicin were purchased from Absin (Shanghai, China). Acrylamide, Muscone, and α-Asarone were from Solarbio (Beijing, China).

FRET probe construction and transfection

NovoRec PCR seamless cloning and assembly kit (Thermo Fisher Scientific) and restriction endonuclease cloning methods were used to construct the FRET-based probes, as described previously[12–15]. The occludin (#86042) and ZO1 (#30313) genes were purchased from Addgene (Watertown, MA, USA). We constructed fluorescent sensors by using the cpstFRET (cpVenus-7aa-cpCerulean) module and inserted them between amino acids 357 and 358 of occludin, and 1011 and 1012 of ZO1. Occludin and ZO1 expression were monitored by inverted fluorescence microscopy. Endo-Free Plasmid Mini Kits (Omega Bio-Tek, Norcross, GA, USA) were used to exact the recombinant FRET plasmids. The FRET plasmids were transfected into HBMEC cells by using the FuGene 6 Transfection Reagent (Roche).

cpstFRET analysis

HBMEC cells were transfected with occludin or ZO1 probes and incubated with 1000 mg/mL geneticin. The effectiveness of FRET in stable monoclonal cell lines depends on the dipole angle between donor-eCFP and acceptor-eYFP. The cell images were taken with × 63 oil lens on a confocal microscope (SP5;

Leica,Wetzlar，Germany). The effectiveness of donor and acceptor were tested using argon lasers at 458 nm and 514 nm respectively. The Eq. 1/E = cerulean donor/venus acceptor was used to calculate the CFP/FRET ratio.

FRET-AB analysis

LAS AF Application Wizard v1.7.0 (Leica) was used to detect the effectiveness of the occludin and ZO1 probes. Acceptor photobleaching FRET (FRET-AB) mode was used after HBMEC cells were transfected with the probes. Donor and receptor exciting light was adjusted to ensure fluorescence intensity of the donor and receptor when the exciting light was as low as possible. The whole cell was selected as the ROI, and the receptor exciting light intensity was adjusted to 100% to bleach the receptor. The ratio of the donor fluorescence intensity before and after bleaching was used to evaluate the FRET-AB efficiency of the probes.

FRAP analysis

Fluorescence recovery after photobleaching (FRAP) experiments were performed using LAS AF Application Wizard v1.7.0 (Leica). The ROI was selected on cells, 458 nm or 514 nm was chosen, and the exciting light intensity was adjusted to 100%. The ratio of fluorescence intensity of ROI before and 500 seconds after photobleaching was used to calculate the FRAP recovery rate of the probes.

Measurement of cytoplasmic OP and count rate of protein particles

Cell culture medium, HEPES isosmotic solution, and trypsin solution were adjusted to 300 ± 10 Osm/kg. HBMEC cells were cultivated in 90 mm dishes and stimulated with drugs when the cell density reached > 95%. Medium was discarded and the cells were washed two times with HEPES isosmotic solution. The cells were digested and suspended in HEPES isosmotic solution and transferred to 1.5 mL microcentrifuge tubes. Centrifugation (13000 *g*, 5 min, 4℃), ultrasonification (75% amplitude, 5 times, 5 seconds; Sonics and Materials, Connecticut, CT, USA) and another centrifugation (13000 g, 10 min, 4℃) were performed. 50 μL of supernatant solution was transferred to 0.5 mL test tubes. The Osmomat 3000 Freezing Point Osmometer and 050 Membrane Osmometer (Gonotec, Berlin, Germany) were calibrated three times before use. The cytoplasmic OP was then recorded. The kilocycles per second (Kcps) of cytoplasmic nanoparticles was detected by Nanosight NS300 (Malvern Instruments, Malvern, UK).

Western blotting

HBMEC cells were dissolved in RIPA lysis buffer (Beyotime Bio) mixed with protease inhibitor and PMSF, and total proteins were extracted. SDS-PAGE was used to separate the proteins. The separated proteins were transferred to nitrocellulose membranes, which were then blocked using 5% non-fat milk for 1 hour. The membranes were incubated with specific primary antibodies overnight at 4 °C. After washing with 0.1% TBST, the membranes were incubated with specific secondary antibodies for 2 hours. The immunoreactive protein bands were visualized using the ECL chromogenic substrate and quantified by densitometry (Quantity One; Bio-Rad,Hercules, CA, USA). Actin or Tubulin were used as negative control.

Measurement of transendothelial electrical resistance in HBMEC cells

An epithelial voltohmmeter (EVOM) was used to record transendothelial electrical resistance (TEER). HBMEC cells were seeded in the transwell apparatus with polycarbonate membrane and cultured with 600 μL DMEM in the upper chamber. The transwell apparatus was placed in a 6-well cell culture cluster and 1 mL DMEM was added into the bottom chamber. After 24 h of incubation, two Millicell® ERS-2 Voltohmmeter electrodes(Merck USA)were placed on the upper and bottom chambers vertically, and immersed in the medium. The TEER value was measured as blank electrical resistance value ($TEER_{blank}$). Glutamate, VEGF, Histamine, or hydrogen peroxide was added into the upper chamber and cells were incubated for 0–90 min; the same volume of PBS was added to the control group. The TEER values in each chamber ($TEER_c$) were measured. The equation ($TEER_c$-$TEER_{blank}$) × S (selective membrane area) = TEER ($\Omega \cdot cm^2$) was used to calculate the TEER values of monolayer cells. For each experiment, at least 2 replicates were measured. Results were expressed as means ± S.E.M.

Animals

All animal procedures were performed according to the guidelines of the National Institutes of Health (Bethesda, MD, USA). The protocol was approved by the Research Animal Care Committee of Nanjing University of Chinese Medicine.

Adult male Sprague-Dawley rats (SD rats, 240–260 g) were obtained from the Model Animal Research Center of Nanjing University of Chinese Medicine (Nanjing, China). The rats were housed in a room under a 12 h light/dark cycle. All rats had free access to food and water under conditions of controlled humidity and temperature (24 ± 0.5℃).

Stereotactic injection in rat brains

The rats were injected with 2% Evans Blue (EB; 4 mL/kg, Sigma-Aldrich, MO, USA) dye dissolved in 0.9% saline solution through the lateral caudal vein. VEGF (5 μg/mL), Glu (20 mM), HP (100 μM), or His (1.25 mM) dissolved in PBS were prepared for injections. Rats were placed in a stereotactic brain frame and anesthetized by administering a mixture of isoflurane (1.5–2.0%) and oxygen by inhalation. A 25-μl Hamilton syringe (Shanghai Gaoge Industry & Trade Co., Ltd., Shanghai, China) was inserted into the right ventricle using the following coordinates: 3.5 mm beside the sagittal suture, 2 mm perforation at the intersection of the coronary suture, and 4 mm insertion. VEGF, Glu, HP, and His were injected into the right ventricle using the 25 μl Hamilton syringe at a rate of 0.5 μl/min. The total volume was 40 μl. The body temperature of rats was controlled at 37.0 ± 0.5 °C using a heating pad.

Evans Blue analysis in the brain

After the stereotactic brain injection cycle, we perfused the heart with 0.9% saline solution for four hours and obtained the brains. We observed and captured images of EB infiltration in the right ventricle of each group. The brain tissue was weighed, and 1 mL of 5% trichloroacetic acid (Sigma-Aldrich, Germany) was

added per 100 g of the brain tissue. The brain was homogenized and sonicated in trichloroacetic acid, and then centrifuged at 13,000 × *g* for 10 minutes. The supernatant was diluted 1 : 4 in 100% ethanol. After incubation for 30 min at room temperature, the obtained sample was transferred to a 96-well black plate (Nunc, USA), and fluorescence emission was measured at 680 nm (excitation wavelength: 620 nm) by using a multifunctional microplate reader (PerkinElmer EnVision, UK).

Measurement of intracellular chloride ions

N-[ethoxycarbonylmethyl]-6-methoxy-quinolinium bromide (MQAE; Beyotime, China) was used to detect intracellular chloride ion concentration. MQAE was dissolved in Krebs-HEPES buffer (PanEra, China). The HBMEC cells were incubated with 5 μM MQAE for 30 min at 37℃, and washed 5 times with Krebs-HEPES buffer. The MQAE fluorescence was excited at 355 nm, and emitted at 460 nm under confocal laser scanning microscopy (SP5; Leica, Wetzlar, Germany). Fluorescence images were obtained every 60 seconds. The fluorescence intensity measured by microscopy was inversely correlated with the chloride ion concentration in HBMEC cells. The normalized value of MQAE fluorescence intensity (F_t/F_0) was calculated using the chloride ion fluorescence just after (F_t) or before (F_0) the application of stimulation for 15 min.

Measurement of intracellular calcium ion

The calcium-sensitive dye Fluo-4 AM (Molecular Probes, Solarbio, China) was used to measure intracellular calcium ion concentration. Fluo-4 AM was dissolved in Hanks balanced salt solution (HBSS) buffer and excited at 494 nm, and emitted at 516 nm. HBMEC cells were incubated with 4 μM Fluo-4 AM for 20 min at 37℃, then treated with 5 times volume HBSS containing 1% FBS and incubated for another 40 min. The cells were resuspended using HEPES buffer saline (10 mM HEPES, 1 mM Na_2PO_4, 137 mM NaCl, 5 mM KCl, 1 mM $CaCl_2$, 0.5 mM $MgCl_2$, 5 mM Glucose, 0.1% BSA, pH 7.4) and incubated for 10 min at 37℃. The fluorescence intensity was detected using a confocal laser scanning microscopy (SP5; Leica, Wetzlar, Germany), and fluorescence images were obtained every 60 seconds. The normalized value of Fluo-4 AM fluorescence intensity (F_t/F_0) was calculated based on the calcium ion fluorescence just after (F_t) or before (F_0) the application of stimulation for 15 min.

Statistical analyses

The CFP/FRET ratio was calculated using ImageJ software (San Diego, CA, USA). The FRET value in each subcellular region was measured for each cell and the average value was calculated for several cells. The 16-color map in ImageJ was used to set pseudo-colors in certain images. Data were presented as mean ± SEM. One-way ANOVA with the least significant difference test was used to determine statistical significance and $P < 0.05$ was considered significant. Each experiment was repeated at least three times, > 10 cells were imaged, and each condition was analyzed.

Results

Construction and efficiency of occludin and ZO1 tension probes

Intracellular tension plays a vital role in the integrity of tight junctions between adjacent brain endothelial cells, and stabilization of the BBB structure, which is closely related to the tight binding of occludin to the cytoskeleton via the scaffold protein ZO1[5, 20]. To determine the role of occludin/ZO1 tension activity in BBB lesions, we designed and constructed FRET-based tension probes of the transmembrane protein occludin and its linking protein ZO1. The FRET module was inserted into the occludin and ZO1 backbones, which could then exhibit resonant energy transfer through angle twisting when bearing tension changes (Fig. 1A). The cpstFRET module was introduced between amino acids 357 and 358 of occludin and 1011 and 1012 of ZO1 (Fig. 1B). HBMEC cells were transfected with the occludin and ZO1 probes, and subjected to the acceptor photobleaching FRET (FRET-AB) test. Donor fluorescence (CFP) increased and acceptor fluorescence (YFP) decreased dramatically during FRET-AB. The FRET efficiency was 17.435% for the occludin probe and 17.02% for the ZO-1 probe (Fig. 1C). The fluorescence recovery after photobleaching (FRAP) test showed that the recovery rate was 28.7% for occludin and 60.3% for ZO1 after 500 seconds (Fig. 1D), suggesting that the fluidity of ZO1 is higher than that of occludin. We then transfected HBMEC cells with occludin-cpstFRET or ZO1-cpstFRET probes under isotonic conditions. Occludin was expressed mainly on the cytomembrane of HBMEC cells and ZO1 was expressed in the surrounding cytoplasm (Figure S1A and Figure S1B). These data suggested that the newly constructed probes were effective and could be used to study intracellular tensions in brain endothelial cells. Further, this would be an effective model to elucidate the mechanical mechanism underlying BBB lesions.

Extracellular BBB lesion stimuli induce occludin and ZO1 tension

Change of BBB structure is closely associated with abnormal intracellular tension in BBB lesions. We therefore studied occludin and ZO1 tension in BBB lesions by using tension probes. VEGF, glutamate (Glu), H_2O_2 (hydrogen peroxide; HP), and histamine (His), which destabilize the BBB and increase its permeability, were used to generate models of BBB damage [21–25]. HBMEC cells were transfected with occludin-cpstFRET or ZO1-cpstFRET probes. Time-lapse imaging of occludin-tension and ZO1-tension were performed and data was presented based on CFP/FRET signals. Occludin tension significantly increased when cells were treated with VEGF or Glu and dramatically decreased when cells were stimulated with HP or His (Fig. 2A and Fig. 2B). Further, ZO1 tension significantly increased in cells treated with VEGF or Glu and dramatically decreased in cells treated with HP or His (Fig. 2C and Fig. 2D). These data showed that occludin and ZO1 tension could be upregulated or downregulated in extracellular BBB lesion models, and the “pulling” or “pushing” of transmembrane proteins elicited by intracellular tension activity could modulate nonselective permeability in the BBB.

Stabilization of cytoskeletal structure limits nonselective permeability of the BBB via increase in intracellular OP in BBB lesion models

Alteration of intracellular OP can also cause structural and functional disruptions in the BBB. Cytoskeletal depolymerization is involved in intracellular OP upregulation, and stabilization and rearrangement of cytoskeletal structure is likely involved in BBB lesions[12, 16, 26]. To determine the tension-related roles of OP in HBMEC cell permeability, a freezing point osmometer was used to measure OP value, and the MT stabilizer taxol (TAX; 15 μM) and MF stabilizer jasplakinolide (JK; 10 μM) were used to block cytoskeletal depolymerization in BBB lesion models. We found that VEGF, Glu, HP, and His stimuli could significantly increase cytoplasmic OP, and TAX and JK pretreatment could dramatically reduce this effect in BBB lesion models (Fig. 3A). We also found that the number of protein nanoparticles induced by VEGF, Glu, HP, or His independently increased dramatically in the BBB lesion models. After treatment with TAX and JK for 15 min, the number of protein nanoparticles was lower than that in cells treated with only BBB lesion factors (Fig. 3B). In addition, we detected the size distribution of protein granules in the cytoplasm. The size distribution of most cytoplasmic particles under normal conditions was > 100 nm, and even > 1000 nm. After treatment with the BBB lesion stimuli VEGF, Glu, HP, or His, monomers of actin or tubulin and macromolecular polymers were produced, and the composition and degree of cytoplasmic OP changed. Treatment with VEGF, Glu, HP, or His resulted in the production of cytoplasmic particles < 100 nm and even < 10 nm. Treatment with stabilizers of MF and MT increased particle size from < 10 nm to 10–100 nm (Fig. 3C). These data suggested that the stabilization of MF and MT could prevent cytoplasmic OP increase in BBB lesion models. Further, the intracellular calcium or chloride ions were measured using Fluo-4 AM or MQAE dyes after stimulation with different drugs for 15 min. Treatment with VEGF, Glu, HP, or His significantly increased the concentration of cytoplasmic calcium or chloride ions, which could be reduced by treatment with stabilizers for MF and MT (Figs. 3D, 3E).

To study the changes of BBB structure and nonselective permeability in BBB models, transendothelial electrical resistance (TEER) was used to assess tight junction formation, and was recorded using a conventional epithelial volt-ohm meter (EVOM); high TEER values indicated low paracellular BBB permeability [27]. We found that treatment with the BBB lesion factors VEGF, Glu, HP, or His could reduce the TEER values in 90 min (Fig. 4A), and cotreatment with the BBB lesion factors and JK and TAX resulted in significantly higher TEER values than those after treatment with only the BBB lesion factors (Fig. 4B). These data suggested that stabilization of cytoskeleton structure could alleviate the increase in BBB permeability induced by BBB lesion stimuli, and could be associated with recovery of intracellular protein nanoparticle osmotic potential.

Cofilin and stathmin are key depolymerization factors for MF and MT respectively[28, 29]. BBB lesioning was correlated with cofilin and stathmin activation elicited by their dephosphorylation. Treatment with the BBB lesion factors VEGF, Glu, HP, or His, could cause significant decreases in p-cofilin or p-stathmin protein levels (Fig. 4C-4F). These data suggested that BBB lesion-related factors could cause cofilin and stathmin activation and subsequent depolymerization of MFs and MTs, which results in mass production of protein nanoparticles and a related increase in OP, associated closely with increased cytoplasmic calcium or chloride ion concentrations.

BBB lesion-factor-induced fluidity of occludin decreases after stabilization of MFs or MTs

Membrane fluidity can have a crucial effect on nonselective permeability of the BBB, which is associated with motion of transmembrane proteins[16, 30]. The fluorescence recovery after photobleaching (FRAP) test was used to study the changes in mobility ratios of the transmembrane protein occludin. The normalized fluorescence recovery ratio after photobleaching after VEGF treatment after 500 s in occludin probe-transfected cells was about 40.1%. The normalized FRAP ratio after treatment with Glu, HP, or His was 46.7%, 55%, and 48%, respectively (Fig. 5A). To further elucidate the roles of stabilizers of MF and MT, we treated occludin probe-transfected VEGF, Glu, HP, or His-induced cellular BBB lesion models with JK and TAX, and observed normalized FRAP ratios of 31.4%, 32.3%, 43.7%, and 38.4% respectively (Fig. 5B). The FRAP ratio was lower after stabilization of cytoskeletal structure than that after treatment with BBB lesion stimuli. These data suggested that recovery of intracellular PN-OP could decrease transmembrane protein fluidity induced by BBB lesion factors after stabilization of MFs or MTs. To elucidate the roles of OP in transmembrane protein fluidity, we treated cells with isotonic, hypotonic, or hypertonic solution, and observed FRAP ratios of 28.7%, 48.97%, and 41.0% respectively. An increase or decrease in OP increased transmembrane protein fluidity (Figure S2A). To determine the roles of stabilizers of MF and MT in different OPs, we treated occludin probe-transfected cells with JK and TAX in isotonic, hypotonic, or hypertonic solution; the normalized FRAP ratios were 28.4%, 34.78%, and 32.48%, respectively. (Figure S2B). These data suggested that the recovery of intracellular OP could decrease transmembrane protein fluidity by stabilization of MFs or MTs, and alteration of protein nanoparticle levels.

Mass production of protein nanoparticles increases occludin and ZO1 tension and BBB permeability in response to cytoskeletal depolymerization

Intracellular OP is closely associated with protein nanoparticle changes. To elucidate the roles of PN-OP in occludin/ZO1 tension, we used cytochalasin D (Cyto D; 10 μM), nocodazole (Noc; 100 μM), and acrylamide (Acr; 2 mM) to depolymerize MFs, MTs and IFs, respectively, which resulted in mass production of protein nanoparticles. Acr, Cyto D, or Noc treatment could significantly increase the occludin tension (Fig. 6A and 6B). The TEER values decreased significantly under treatment with only Acr, Cyto D, or Noc, and cotreatment with all three depolymerizers (Fig. 6C). Similarly, treatment with Acr, Cyto D, and Noc individually or together could significantly increase ZO1 tension. Cotreatment with Acr, Cyto D, and Noc could increase the ZO1 tension much more than treatment with each individual depolymerizer could (Fig. 6D and 6E). The TEER values also decreased dramatically after treatment with Acr, Cyto D, or Noc individually or together (Fig. 6F). FRAP tests were performed to determine the fluidity of occludin after cytoskeleton depolymerization in isotonic solution. We treated occludin probe-transfected cells with Acr, Cyto D, Noc, and Cyto D and Noc; the normalized FRAP ratios were 36.9%, 34.8%, 40.6%, and 47.2%, respectively. The normalized FRAP ratio increased significantly compared with the control group, in which the FRAP ratio was 28.7% (Fig. 6G). These data suggested that mass protein nanoparticle production

could increase occludin/ZO1 tension and augment the permeability of the BBB in response to cytoskeleton depolymerization, which is closely related to intracellular OP increase.

Protein nanoparticle downregulation plays a role in regulation of occludin tension in response to BBB lesion stimuli

Stabilization of cytoskeletal structure could effectively attenuate intracellular protein nanoparticle production and the related OP. To determine the effects of PN on occludin tension in BBB lesions, MF and MT stabilizers were used to restore intracellular PN levels in cellular BBB lesion models. Occludin tension after cotreatment with stabilizers of MF and MT and VEGF was significantly lower than that after VEGF treatment only (Fig. 7A and 7B). Treatment with only JK and TAX did not affect the occludin tension (Fig. 7A and 7B). Treatment with JK, TAX, and Glu caused a dramatic decrease in occludin tension compared to treatment with Glu only (Fig. 7A and 7C). We then studied the roles of HP and His in occludin tension. Interestingly, cotreatment with JK and TAX could significantly increase occludin tension in response to HP or His stimulation (Fig. 7D, 7E, and 7F).

These data suggested that reduction of intracellular protein nanoparticles is involved in the recovery of occludin tension in BBB lesion models, and PN-OP modulates the permeability of the BBB via tension activity of tight junctions.

Inhibition of PN production could block nonselective BBB permeability in vivo

In order to clarify the role of intracellular PN in BBB permeability *in vivo*, MF and MT stabilizers were used to restore intracellular PN levels in an adult male SD rat BBB lesion model; the schematic diagram of the experiment is shown in Fig. 7A[31, 32]. The SD rats were injected with Evans Blue (EB). The changes in EB content could be used to determine BBB permeability *in vivo*[33–35]. The body of the rats, including the eyes, ears, and feet turned blue (Fig. 8B). After EB injection, VEGF, Glu, HP, and His dissolved in PBS were injected into the rat brains and PBS was injected as a control. The four BBB lesion factors significantly promoted BBB lesioning in the rat brain relative to the control. After treatment with the cytoskeleton stabilizers JK and TAX, the nonselective permeability of the BBB in rat brain reduced dramatically (Fig. 8C). Quantitative analysis of EB extravasation in the coronal section of rat brain confirmed this result (Fig. 8F). The EB standard curve was calculated using the following equation: Y = 0.00796X + 0.03398 (Fig. 8D). The EB exosmosis from brain tissues was calculated using the equation. The four BBB lesion factors significantly increased EB exosmosis, and treatment with JK and TAX could reduce the EB concentration (Fig. 8E).

Overall, these data indicated that inhibition of PN production could inhibit the nonselective permeability of the BBB via downregulation of OP in *in vivo* model.

Select herb extracts augment the permeability of the BBB by increasing protein nanoparticle-induced OP

Based on the Gibbs-Donnan equilibrium, we hypothesized a vital role for protein nanoparticle-induced osmotic pressure (PN-OP) in BBB injury [12, 36]. To elucidate the molecular mechanisms underlying PN-OP-related changes in BBB permeability, we studied the impact of various stimuli or herbs and their effective concentrations on the ion osmotic pressure (IOP) and PN-OP in HBMEC cells. We screened several herb extracts and selected Capsaicin, Borneol, Muscone, and α-Asarone, which could improve BBB permeability for subsequent experiments[37–42]. The cytoplasmic osmotic pressure and the number of protein nanoparticles significantly increased when cells were treated with these compounds (Fig. 9A). We also studied the size distribution of cytoplasmic nanoparticles. Cytoplasmic granules were smaller in size, and the number of nanoparticles significantly higher (Fig. 9B) after treatment with the herbal compounds. Intracellular calcium and chloride ion concentrations were measured using Fluo-4 AM dye and MQAE tests over 15 min. The cytoplasmic calcium (Fig. 9C) and chloride (Fig. 9D) ions concentrations were significantly higher in the herbs-treated groups than in the control group.

In summary, augmentation of PN-OP is a common mechanism underlying BBB lesion elicited by various herb extracts, and could mediate BBB permeability. PN-OP is also closely associated with intracellular ion increase, especially of calcium ions.

Discussion

Intracellular tension activity plays a vital role in structural and functional changes of the BBB; abnormal tension activity could contribute to BBB breakdown or dysfunction, and is associated with several degenerative neurological diseases such as stroke, Alzheimer's disease, Parkinson's disease, and glioblastoma[43]. In this study, we found that BBB lesions were caused by increased cytoplasmic protein nanoparticle OP (PN-OP) and changes in occludin/ZO1 tension. Blocking of abnormal tension activity could reduce membrane fluidity and nonselective drug influx, suggesting that intracellular tension activity plays an essential role in BBB dysfunction.

Intracellular osmotic pressure could be regulated by protein nanoparticle production, as suggested by the Donnan effect, according to which, under physiological pH conditions, protein nanoparticles such as actin and α/β-tubulin carry negative charges and mainly adsorb cytoplasmic cations (such as K^+) thereby inducing extracellular cation (mainly Na^+) influx. The accumulation of cations causes a charge gradient, leading to the influx of negative ions and eventually intracellular hyperosmolarity[12, 44, 45]. However, in the human blood, albumin protein nanoparticles have few effects on OP regulation in the plasma. The results of our recent studies suggested an explanation for the divergence between intra and extracellular PN-OP and indicated that calcium ions are essential for intracellular PN-OP tension. Calcium ions and PN synergistically modulate the tension effect of PN-OP according the double electric layer theory[46, 47]. Data from the present study also indicate that PN-OP elicited by BBB lesion factors is accompanied by an increase in calcium ions. The role of divalent calcium ion in PN-OP could indicate a novel mechanism underlying human OP.

Intracellular protein nanoparticle-related osmotic pressure was closely associated with BBB lesions. Some synthetic or natural compounds that promote the permeability of the blood-brain barrier can increase cytoplasmic ion concentration and mass protein nanoparticle production in endothelial cells. Further, MF and MT stabilization could reduce BBB lesion-factor-induced increase of ion concentration and OP. Moreover, activation of depolymerization factors is crucial for the upregulation of intracellular ion content and OP, and contributes to BBB lesion. Finally the antagonistic roles of MF and MT stabilization in the pathological changes of BBB permeability have been observed in *in vivo* models. Intracellular protein nanoparticle-induced osmotic potential, a crucial tension factor, could play an important role in the regulation of nonselective BBB permeability, in accordance with previous studies that hyperosmotic stimuli could result effectively in blood-brain barrier opening (OBBBO) or disruption [51, 52].

The transmembrane protein occludin and cytoplasmic attachment protein ZO1 are the main structural proteins of tight junctions (TJ), and have different tension distributions. Microfilament and microtubule pulling tensions could cause occludin/ZO1 tension.[13, 48] The results of this study suggest that the intracellular PN-OP is essential for alteration of occludin/ZO1 tension. Recovery of PN-OP could effectively reverse the changes in occludin/ZO1 tension, which is closely associated with intracellular controllable tension activities (such as OP, MF, and MT forces) and their interactions. In addition, intracellular occludin/ZO1 tension changed after the treatment with different BBB lesion factors, indicating that occludin/ZO1 tension is involved in BBB function, and could be an indirect factor affecting BBB permeability. Thus, intracellular tension and the associated interactions are necessary to maintain normal BBB structure and function.

Upregulation of membrane fluidity promotes nonselective drugs influx. The rapid membrane flow is characterized by the fluidity of lipids and transmembrane proteins. Membrane fluidity is regulated by the composition of fatty acids, and by cytoskeletal pull of cytoskeletons, which maintains and stabilizes the connections between transmembrane proteins and cytoskeleton tension[49, 50]. OP was thought to be involved in the regulation of membrane fluidity: changes in extracellular OP increased membrane fluidity. Hyperosmosis and hypoosmolality could promote membrane fluidity associated with MF and MT depolymerization (sFig.2). Further, the recovery of intracellular OP due to cytoskeleton stabilization decreased transmembrane protein fluidity by cytoskeleton reorganization and recovery of intracellular OP (Fig. 5). Moreover, PN-OP elicited by cytoskeleton depolymerization also plays a role in occludin/ZO1 tension; different sources of tension including MF and MT forces, osmotic potential, and transmembrane protein tension function reciprocally in the regulation of membrane fluidity (Fig. 6G). Our data support the hypothesis that PN-OP plays a vital role in BBB nonselective permeability via the regulation of plasma membrane fluidity.

We also screened herb extracts that can promote BBB permeability, such as borneol, musk ketone, α-asarone, and capsaicin, which shared similar mechanisms of BBB permeability modulation, caused a clear increase in intracellular PN-OP, and upregulated intracellular calcium and chloride ion levels to various degrees. Thus, upregulation of intracellular osmotic potential energy due to increased intracellular

protein nanoparticles, divalent ions, and PN-OP could form a mechanism by which BBB non-selective permeability is regulated.

Conclusions

In conclusion, the results of this study suggested that intracellular tension activity is involved in BBB disruption, and the tight junction structure could be modulated by tension activity. However, increase of intracellular osmotic pressure played crucial roles in changing BBB permeability, likely owing to the depolymerization of MFs or MTs and mass production of protein nanoparticles based on the Donnan effect, particularly associated with divalent calcium ions. The outward tension of intracellular osmotic potential also induced upregulation of membrane fluidity and promoted nonselective drug influx. Our results suggest a crucial mechanical mechanism underlying BBB lesions, and protein nanoparticle osmotic pressure could be a novel therapeutic target for BBB lesion-related brain diseases. Our results also provide a basis for further studies on the regulation of intracellular tension activity and its effect on the permeability of the BBB, and development of novel drugs that cross the blood-brain barrier.

Abbreviations

BBB
Blood brain barrier; TJ:Tight junction; MF:Microfilament; MT:Microtubule; OP:Osmotic pressure; IF:Intermediate filament; FRET:Fluorescence resonance energy transfer; cpstFRET:cpVenus-7aa-cpCerulean; FRET-AB:FRET acceptor photobleaching; FRAP:Fluorescence recovery after photobleaching; ROI:Ratio of fluorescence intensity; HBMEC:Human brain microvascular endothelial cell; BNCC:BeNa Culture Collection; STR:Short tandem repeats; Kcps:Kilocycles per second; PN:Protein nanoparticle; PN-OP:Protein nanoparticle-induced osmotic pressure; IOP:Ion osmotic pressure; EVOM:Epithelial voltohmmeter; TEER:Transendothelial electrical resistance; $TEER_{blank}$:Blank electrical resistance value; $TEER_c$:TEER values in each chamber; SD rats:Sprague-Dawley rats; EB:Evans Blue; MQAE:N-[ethoxycarbonylmethyl]-6-methoxy-quinolinium bromide; HBSS:Hanks balanced salt solution; VEGF:Vascular endothelial growth factor; Glu:Glutamate; His:Histamine; HP:Hydrogen peroxide, H_2O_2; TAX:Taxol; JK:Jasplakinolide; Cyto D:Cytochalasin D; Noc:Nocodazole; Acr:Acrylamide; OBBBO:Blood-brain barrier opening; LPS:Lipopolysaccharides; TNF-α:Tumor necrosis factor α; Ang-□:Angiogenin-□; ECL:Efficient chemiluminescence.

Declarations

Ethics Approval and consent to participate

Not applicable.

Consent for Publication

Not applicable.

Availability of supporting data.

Not applicable.

Competing interests

The authors declare that they have no competing interests.

Funding

This research was supported by Grants from National Natural Science Foundation of China (No.81573409), Key Program of Natural Science Foundation of Jiangsu Province (No.19KJA320003) and a Project Funded by the Priority Academic Program Development of Jiangsu Higher Education Institutions (Integration of Traditional Chinese and Western Medicine).

Authors' contributions

Jun Guo conceived the experiment, Chen Li, LinLin Chen, YuanYuan Wang, TingTing Wang, Dong Di and HuanHuan Zhao performed the experiments. Chen Li, LinLin Chen and Xu Shen analyzed and interpreted the data, Chen Li, LinLin Chen and Hao Zhang wrote the manuscript. All authors read and approved the final manuscript.

Acknowledgements

Not applicable.

References

[1] Tam SJ, Watts RJ. Connecting vascular and nervous system development: angiogenesis and the blood-brain barrier. Annu Rev Neurosci. 2010 Apr; 33:379-408.

[2] Auvity S, Caille F, Marie S, Wimberley C, Bauer M, Langer O, Buvat I, Goutal S, Tournier N. P-Glycoprotein (ABCB1) Inhibits the Influx and Increases the Efflux of (11)C-Metoclopramide Across the Blood-Brain Barrier: A PET Study on Nonhuman Primates. J Nucl Med. 2018 Oct; 59(10):1609-1615.

[3] Perez-Alvarez A, Navarrete M, Covelo A, Martin ED, Araque A. Structural and functional plasticity of astrocyte processes and dendritic spine interactions. J Neurosci. 2014 Sep; 34(38):12738-12744.

[4] Fleegal-Demotta MA, Doghu S, Banks WA. Angiotensin II modulates BBB permeability via activation of the AT(1) receptor in brain endothelial cells. J Cereb Blood Flow Metab. 2009 Mar; 29(3):640-647.

[5] Tietz S, Engelhardt B. Brain barriers: Crosstalk between complex tight junctions and adherens junctions. J Cell Biol. 2015 May; 209(4):493-506.

[6] Liu J, Jin X, Liu KJ, Liu W. Matrix metalloproteinase-2-mediated occludin degradation and caveolin-1-mediated claudin-5 redistribution contribute to blood-brain barrier damage in early ischemic stroke stage. J Neurosci. 2012 Feb; 32(9):3044-3057.

[7] Leng X, Ma J, Liu Y, Shen S, Yu H, Zheng J, Liu X, Liu L, Chen J, Zhao L, Ruan X, Xue Y. Mechanism of piR-DQ590027/MIR17HG regulating the permeability of glioma conditioned normal BBB. J Exp Clin Cancer Res. 2018 Oct; 37(1):246.

[8] Du D, Xu F, Yu L, Zhang C, Lu X, Yuan H, Huang Q, Zhang F, Bao H, Jia L, Wu X, Zhu X, Zhang X, Zhang Z, Chen Z. The tight junction protein, occludin, regulates the directional migration of epithelial cells. Dev Cell. 2010 Jan; 18(1):52-63.

[9] Torii H, Kubota H, Ishihara H, Suzuki M. Cilostazol inhibits the redistribution of the actin cytoskeleton and junctional proteins on the blood-brain barrier under hypoxia/reoxygenation. Pharmacol Res. 2007 Feb; 55(2):104-110.

[10] Kneussel M,Wagner W. Myosin motors at neuronal synapses: drivers of membrane transport and actin dynamics. Nat Rev Neurosci. 2013 Apr; 14(4):233-247.

[11] Hirokawa N, Niwa S,Tanaka Y. Molecular motors in neurons: transport mechanisms and roles in brain function, development, and disease. Neuron. 2010 Nov; 68(4):610-638.

[12] Zhang J, Wang Y, Zheng Z, Sun X, Chen T, Li C, Zhang X, Guo J. Intracellular ion and protein nanoparticle-induced osmotic pressure modify astrocyte swelling and brain edema in response to glutamate stimuli. Redox Biol. 2019 Feb; 21: 101112.

[13] Chen T, Guo Y, Shan J, Zhang J, Shen X, Guo J, Liu XM. Vector Analysis of Cytoskeletal Structural Tension and the Mechanisms that Underpin Spectrin-Related Forces in Pyroptosis. Antioxid Redox Signal. 2019 Apr; 30(12):1503-1520.

[14] Wang Y, Zhang X, Tian J, Shan J, Hu Y, Zhai Y, Guo J. Talin promotes integrin activation accompanied by generation of tension in talin and an increase in osmotic pressure in neurite outgrowth. FASEB J. 2019 May; 33(5):6311-6326.

[15] Zhang X, Li G, Guo Y, Song Y, Chen L, Ruan Q, Wang Y, Sun L, Hu Y, Zhou J, Ren B, Guo J. Regulation of ezrin tension by S-nitrosylation mediates non-small cell lung cancer invasion and metastasis. Theranostics. 2019 Apr; 9(9):2555-2571.

[16] Schultz ML, Tecedor L, Lysenko E, Ramachandran S, Stein CS, Davidson BL. Modulating membrane fluidity corrects Batten disease phenotypes in vitro and in vivo. Neurobiol Dis. 2018 Jul; 115:182-193.

[17] Orthmann A, Zeisig R, Koklic T, Sentjurc M, Wiesner B, Lemm M, Fichtner I. Impact of membrane properties on uptake and transcytosis of colloidal nanocarriers across an epithelial cell barrier model. J Pharm Sci. 2010 May; 99(5):2423-2433.

[18] Guo YC, Wang YX, Ge YP, Yu LJ, Guo J. Analysis of subcellular structural tension in axonal growth of neurons. Rev Neurosci. 2018 Feb; 29(2):125-137.

[19] Yang C, Zhang X, Guo Y, Meng F, Sachs F, Guo J. Mechanical dynamics in live cells and fluorescence-based force/tension sensors. Biochim Biophys Acta. 2015 Aug; 1853(8):1889-1904.

[20] Tornavaca O, Chia M, Dufton N, Almagro LO, Conway DE, Randi AM, Schwartz MA, Matter K, Balda MS. ZO-1 controls endothelial adherens junctions, cell-cell tension, angiogenesis, and barrier formation. J Cell Biol. 2015 Mar; 208(6):821-838.

[21] Ba J, Peng H, Chen Y, Gao Y. Effects and mechanism analysis of vascular endothelial growth factor and salvianolic acid B on 125I-low density lipoprotein permeability of the rabbit aortary endothelial cells. Cell Biochem Biophys. 2014 Dec; 70(3):1533-1538.

[22] Wu L, Ye Z, Pan Y, Li X, Fu X, Zhang B, Li Y, Lin W, Li X, Gao Q. Vascular endothelial growth factor aggravates cerebral ischemia and reperfusion-induced blood-brain-barrier disruption through regulating LOC102640519/HOXC13/ZO-1 signaling. Exp Cell Res. 2018 Aug; 369(2):275-283.

[23] Kaneko Y, Pappas C, Malapira T, Vale FL, Tajiri N, Borlongan CV. Extracellular HMGB1 Modulates Glutamate Metabolism Associated with Kainic Acid-Induced Epilepsy-Like Hyperactivity in Primary Rat Neural Cells. Cell Physiol Biochem. 2017 Feb; 41(3):947-959.

[24] Jiang Z, Wang W,Guo C. Tetrahydroxy stilbene glucoside ameliorates H2O2-induced human brain microvascular endothelial cell dysfunction in vitro by inhibiting oxidative stress and inflammatory responses. Mol Med Rep. 2017 Oct; 16(4):5219-5224.

[25] Srinivas SP, Satpathy M, Guo Y, Anandan V. Histamine-induced phosphorylation of the regulatory light chain of myosin II disrupts the barrier integrity of corneal endothelial cells. Invest Ophthalmol Vis Sci. 2006 Sep; 47(9):4011-4018.

[26] Kozler P, Riljak V, Pokorny J. Both water intoxication and osmotic BBB disruption increase brain water content in rats. Physiol Res. 2013 May; 62 Suppl 1:S75-S80.

[27] Buzza MS, Martin EW, Driesbaugh KH, Desilets A, Leduc R, Antalis TM. Prostasin is required for matriptase activation in intestinal epithelial cells to regulate closure of the paracellular pathway. J Biol Chem. 2013 Apr; 288(15):10328-10337.

[28] Byrne FL, Yang L, Phillips PA, Hansford LM, Fletcher JI, Ormandy CJ, Mccarroll JA, Kavallaris M. RNAi-mediated stathmin suppression reduces lung metastasis in an orthotopic neuroblastoma mouse model. Oncogene. 2014 Feb; 33(7):882-890.

[29] Bielig H, Lautz K, Braun PR, Menning M, Machuy N, Brugmann C, Barisic S, Eisler SA, Andree M, Zurek B, Kashkar H, Sansonetti PJ, Hausser A, Meyer TF, Kufer TA. The cofilin phosphatase slingshot homolog 1 (SSH1) links NOD1 signaling to actin remodeling. PLoS Pathog. 2014 Sep; 10(9):e1004351.

[30] Matsuzaki T, Matsumoto S, Kasai T, Yoshizawa E, Okamoto S, Yoshikawa HY, Taniguchi H, Takebe T. Defining Lineage-Specific Membrane Fluidity Signatures that Regulate Adhesion Kinetics. Stem Cell Reports. 2018 Oct; 11(4):852-860.

[31] Grkovski M, Kohutek ZA, Schoder H, Brennan CW, Tabar VS, Gutin PH, Zhang Z, Young RJ, Beattie BJ, Zanzonico PB, Huse JT, Rosenblum MK, Blasberg RG, Humm JL, Beal K. (18)F-Fluorocholine PET uptake correlates with pathologic evidence of recurrent tumor after stereotactic radiosurgery for brain metastases. Eur J Nucl Med Mol Imaging. 2020 Jun; 47(6):1446-1457.

[32] Tejedor LS, Wostradowski T, Gingele S, Skripuletz T, Gudi V, Stangel M. The Effect of Stereotactic Injections on Demyelination and Remyelination: a Study in the Cuprizone Model. J Mol Neurosci. 2017 Apr; 61(4):479-488.

[33] Riabinska A, Zille M, Terzi MY, Cordell R, Nieminen-Kelha M, Klohs J, Pina AL. Pigment Epithelium-Derived Factor Improves Paracellular Blood-Brain Barrier Integrity in the Normal and Ischemic Mouse Brain. Cell Mol Neurobiol. 2020 Jul; 40(5):751-764.

[34] Hou ST, Nilchi L, Li X, Gangaraju S, Jiang SX, Aylsworth A, Monette R, Slinn J. Semaphorin3A elevates vascular permeability and contributes to cerebral ischemia-induced brain damage. Sci Rep. 2015 Jan; 5:7890.

[35] Shim KH, Jeong KH, Bae SO, Kang MO, Maeng EH, Choi CS, Kim YR, Hulme J, Lee EK, Kim MK, An SS. Assessment of ZnO and SiO2 nanoparticle permeability through and toxicity to the blood-brain barrier using Evans blue and TEM. Int J Nanomedicine. 2014 Dec; 9 Suppl 2:225-233.

[36] Lang GE, Stewart PS, Vella D, Waters SL, Goriely A. Is the Donnan effect sufficient to explain swelling in brain tissue slices? J R Soc Interface. 2014 Jul; 11(96):20140123.

[37] Chen ZZ, Lu Y, Du SY, Shang KX, Cai CB. Influence of borneol and muscone on geniposide transport through MDCK and MDCK-MDR1 cells as blood-brain barrier in vitro model. Int J Pharm. 2013 Nov; 456(1):73-79.

[38] Huber G, Schuster F, Raasch W. Brain renin-angiotensin system in the pathophysiology of cardiovascular diseases. Pharmacol Res. 2017 Nov; 125(Pt A):72-90.

[39] Boitsova EB, Morgun AV, Osipova ED, Pozhilenkova EA, Martinova GP, Frolova OV, Olovannikova RY, Tohidpour A, Gorina Y V, Panina Y A, Salmina A B. The inhibitory effect of LPS on the expression of GPR81 lactate receptor in blood-brain barrier model in vitro. J Neuroinflammation. 2018 Jul; 15(1):196.

[40] Wang K, Wang H, Lou W, Ma L, Li Y, Zhang N, Wang C, Li F, Awais M, Cao S, She R, Fu ZF, Cui M. IP-10 Promotes Blood-Brain Barrier Damage by Inducing Tumor Necrosis Factor Alpha Production in Japanese Encephalitis. Front Immunol. 2018 May; 9:1148.

[41] Kaiser M, Burek M, Britz S, Lankamp F, Ketelhut S, Kemper B, Forster C, Gorzelanny C, Goycoolea FM. The Influence of Capsaicin on the Integrity of Microvascular Endothelial Cell Monolayers. Int J Mol Sci. 2018 Dec; 20(1):122.

[42] Wu JY, Li YJ, Yang L, Hu YY, Hu XB, Tang TT, Wang JM, Liu XY, Xiang DX. Borneol and Alpha-asarone as adjuvant agents for improving blood-brain barrier permeability of puerarin and tetramethylpyrazine by activating adenosine receptors. Drug Deliv. 2018 Nov; 25(1):1858-1864.

[43] Zhao Z, Nelson AR, Betsholtz C, Zlokovic BV. Establishment and Dysfunction of the Blood-Brain Barrier. Cell. 2015 Nov; 163(5):1064-1078.

[44] Kinoshita R, Ishima Y, Chuang V, Nakamura H, Fang J, Watanabe H, Shimizu T, Okuhira K, Ishida T, Maeda H, Otagiri M, Maruyama T. Improved anticancer effects of albumin-bound paclitaxel nanoparticle via augmentation of EPR effect and albumin-protein interactions using S-nitrosated human serum albumin dimer. Biomaterials. 2017 Sep; 140:162-169.

[45] Elkin BS, Shaik MA,Morrison BR. Fixed negative charge and the Donnan effect: a description of the driving forces associated with brain tissue swelling and oedema. Philos Trans A Math Phys Eng Sci. 2010 Feb; 368(1912):585-603.

[46] Zheng ZH, Chen JH, Qiu HM, Xie Q, Zhang JR, Zhao HH, Guo J. Divalent cations control protein nanoparticle-induced osmotic pressure and water flux in live cells. Science Advances.

[47] Lin S, Xu L, Chi WA, Wang ZL. Quantifying electron-transfer in liquid-solid contact electrification and the formation of electric double-layer. Nat Commun. 2020 Jan ; 11(1):399.

[48] Niessen CM. Tight junctions/adherens junctions: basic structure and function. J Invest Dermatol. 2007 Nov; 127(11):2525-2532.

[49] Degreif D, de Rond T, Bertl A, Keasling JD, Budin I. Lipid engineering reveals regulatory roles for membrane fluidity in yeast flocculation and oxygen-limited growth. Metab Eng. 2017 May; 41:46-56.

[50] Holguin SY, Anderson CF, Thadhani NN, Prausnitz MR. Role of cytoskeletal mechanics and cell membrane fluidity in the intracellular delivery of molecules mediated by laser-activated carbon nanoparticles. Biotechnol Bioeng. 2017 Oct; 114(10):2390-2399.

[51] Rapoport SI. Advances in osmotic opening of the blood-brain barrier to enhance CNS chemotherapy. Expert Opinion on Investigational Drugs. 2001; 10(10):1809-1818.

[52] Chu CY, Jablonska A, Lesniak WG, Thomas AM, Lan XY, Linville RM, Li S, Searson PC, Liu GS, Pearl M, Pomper MG, Janowski M, Magnus T, Walczak P. Optimization of osmotic blood-brain barrier opening to enable intravital microscopy studies on drug delivery in mouse cortex. Journal of Controlled Release. 2020 Jan; 317: 312-321.

Figures

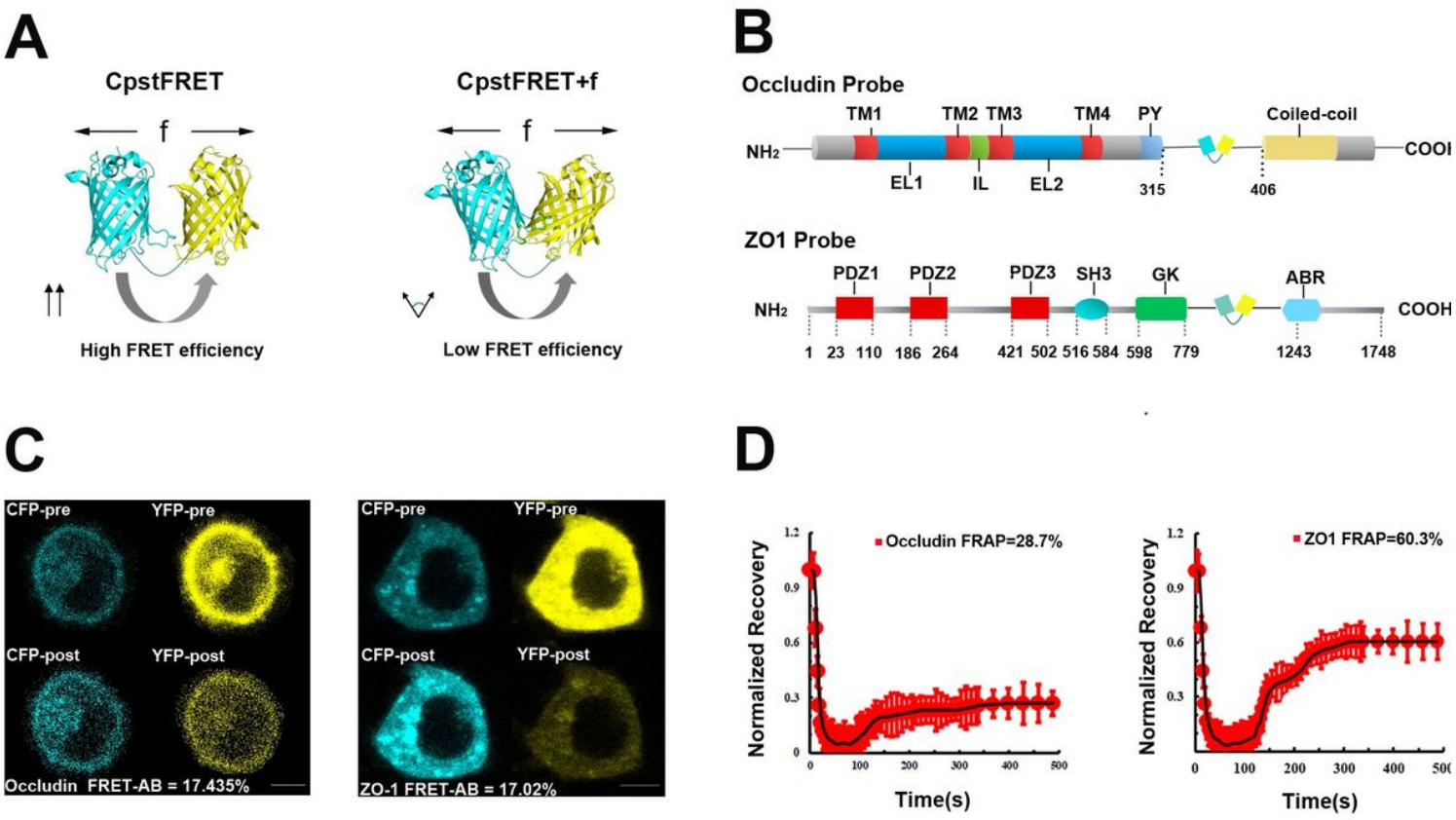

Figure 1

Construction of occludin/ZO1 probes and analysis of their efficacy and motility A. In cpstFRET (cpVenus-7aa-cpCerulean), cpCerulean (cyan) is the donor and cpVenus (yellow) is the acceptor. The probes have high Förster resonance energy transfer (FRET) efficiency when donor and acceptor are parallel without external force (f: external force). The external force reduces the FRET efficiency by changing the angle of cpstFRET. B. Schematic representation of the occludin/ZO1 probe constructs. The cpstFRET module was inserted between amino acids 357 and 358 in the occludin probe and amino acids 1011 and 1012 in the ZO1 probe. C. FRET acceptor photobleaching (FRET-AB) was used to test the efficacy of the occludin (left) and ZO1 (right) probes in HBMEC cells. FRET-AB efficiency was 17.435% for the occludin probe and 17.02% for the ZO1 probe. D. The intracellular mobility of the occludin (left) and ZO1 probes (right) were determined using fluorescence recovery after photobleaching (FRAP). The normalized average fluorescence recovery of occludin (left) and ZO1 (right) vs. time (500 s) was calculated (n = 8), and the fluorescence recovery ratio noted. Scale bar: 20 μm.

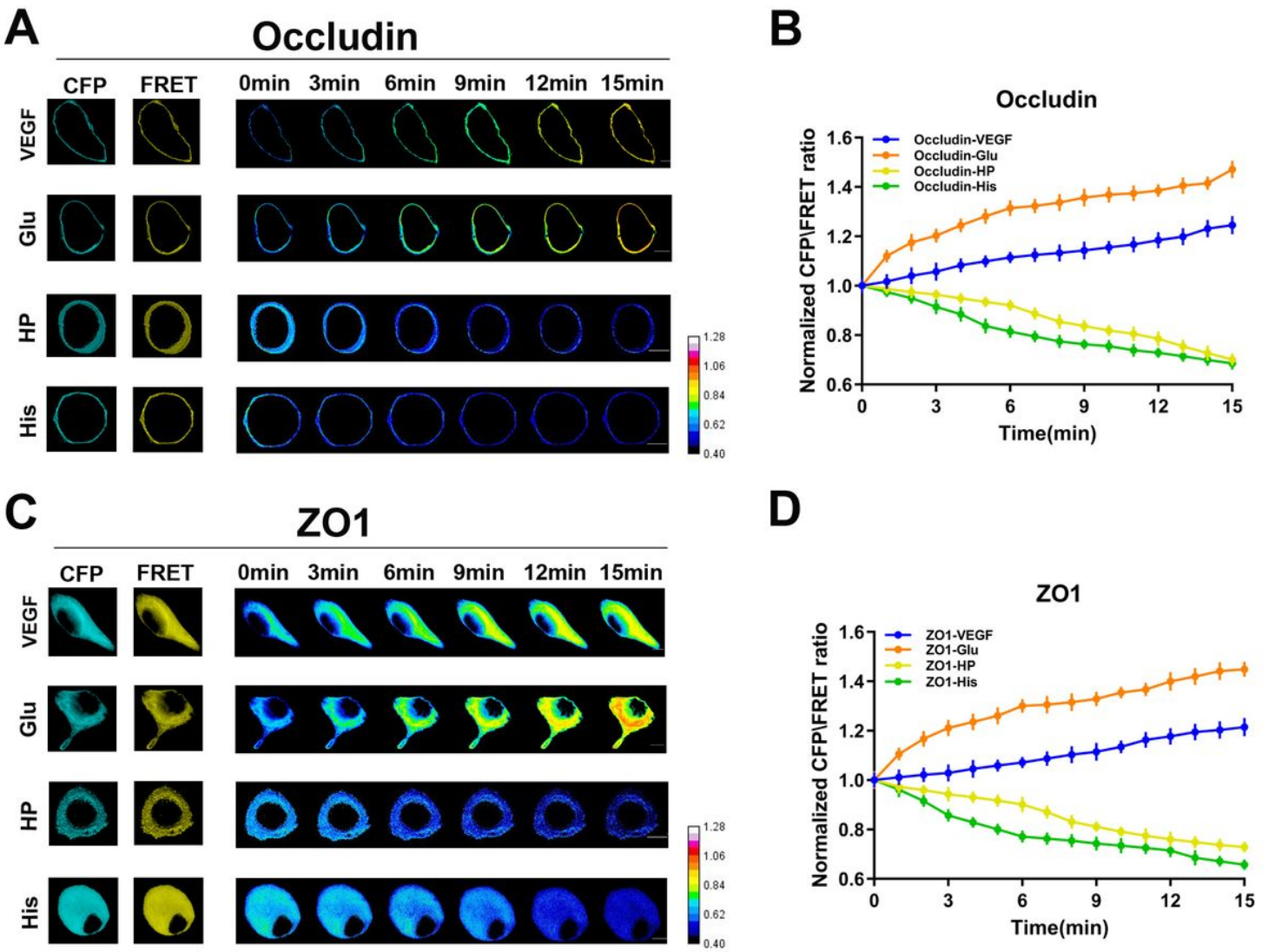

Figure 2

Occludin/ ZO1 tension was regulated after stimulation with VEGF, Glu, HP, and His A and C. HBMEC cells expressing occludin (A) or ZO1 (C) probe were treated with VEGF (row 1), Glu (row 2), HP (row 3), or His (row 4) for 15 min. CFP (cyan) and FRET (yellow) fluorescence images were processed using the 16-color map of Image J. The calibration bar was set from 0.40 to 1.28. Scale bar: 20 μm. B and D. Normalization of CFP/FRET signals corresponding to occludin/ZO1-tension vs. time under VEGF, Glu, HP, and His stimulation. Data are shown as mean ± SEM，n ≥ 5.

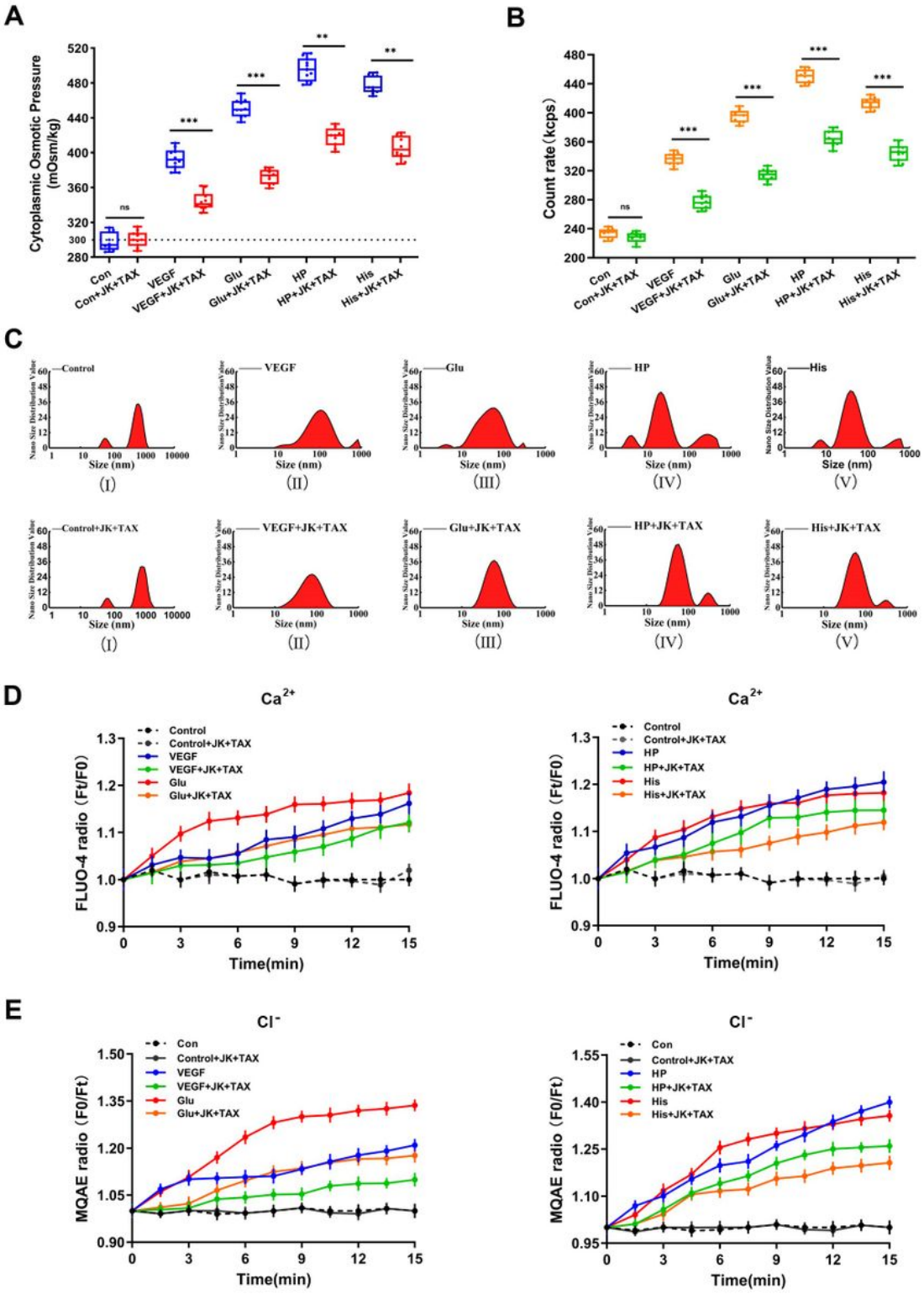

Figure 3

Changes in intracellular protein nanoparticle-induced osmotic pressure and intracellular ions in response to BBB lesion factors and treatment with cytoskeleton stabilizers. A and B. Cytoplasmic osmotic pressure (A) and number of protein nanoparticles (B) in HBMEC cells in response to VEGF, Glu, His, HP, VEGF+JK+TAX, Glu+JK+TAX, HP+JK+TAX, and His+JK+TAX stimulation for 15 min. C. Protein nanoparticle size distribution in the cytoplasm of HBMEC cells after treatment with VEGF, Glu, HP, and His

(Top □-□), or VEGF+JK+TAX, Glu+JK+TAX, HP+JK+TAX, and His+JK+TAX (Bottom □-□) for 15 min. D. Changes in fluorescence intensity of cytoplasmic calcium ions in HBMEC cells. Con, VEGF, VEGF+JK+TAX, Con, HP, and HP+JK+TAX treated groups are on the left, and Glu, Glu+JK+TAX, His, and His+JK+TAX treated groups are on the right. E. Changes in intracellular chloride ion fluorescence intensity in HBMEC cells. Con, VEGF, VEGF+JK+TAX, Con, HP, and HP+JK+TAX treated groups are on the left and Glu, Glu+JK+TAX, His, and His+JK+TAX treated groups are on the right. Data are presented as mean ± SEM□n ≥ 5.

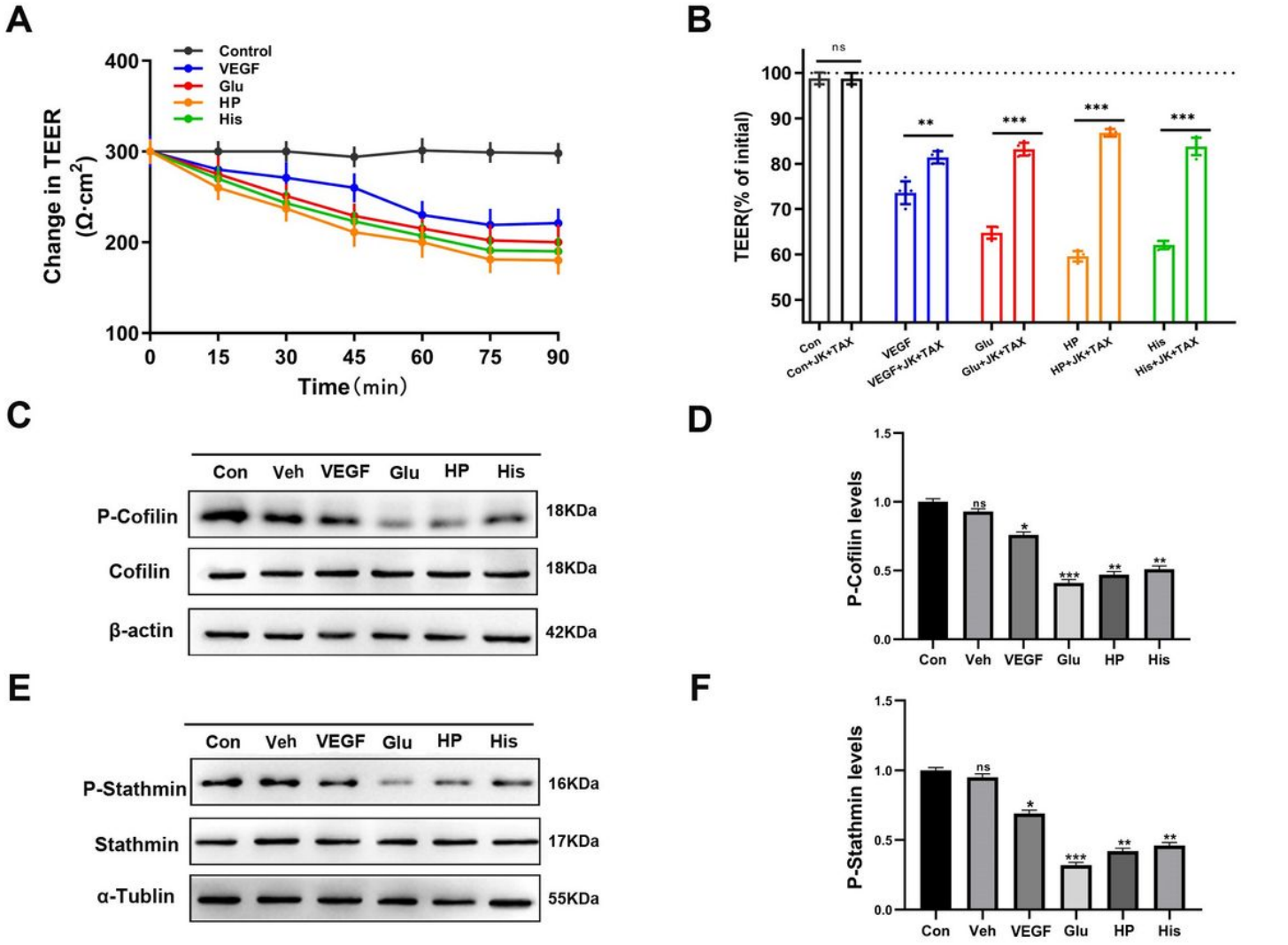

Figure 4

Changes in BBB permeability after treatment of BBB lesion factors and cytoskeleton stabilizers. A. Changes in TEER (Ω▪cm2) values in HBMEC cells vs. time (90 min) after treatment with VEGF, Glu, HP, and His. HBMEC cells were treated with VEGF, VEGF+JK+TAX, Glu, Glu +JK+TAX, HP, HP +JK+TAX, His, and His +JK+TAX for 90 min. B. Normalized TEER values of each group; TEER value measured in control group was defined as 100%. C and E. Western blot analysis to determine the dephosphorylation levels of

(C) cofilin and (E) stathmin induced by VEGF, Glu, HP, and His. D and F. Normalization of (D) P-Cofilin and (F) P-Stathmin levels induced by VEGF, Glu, HP, and His.

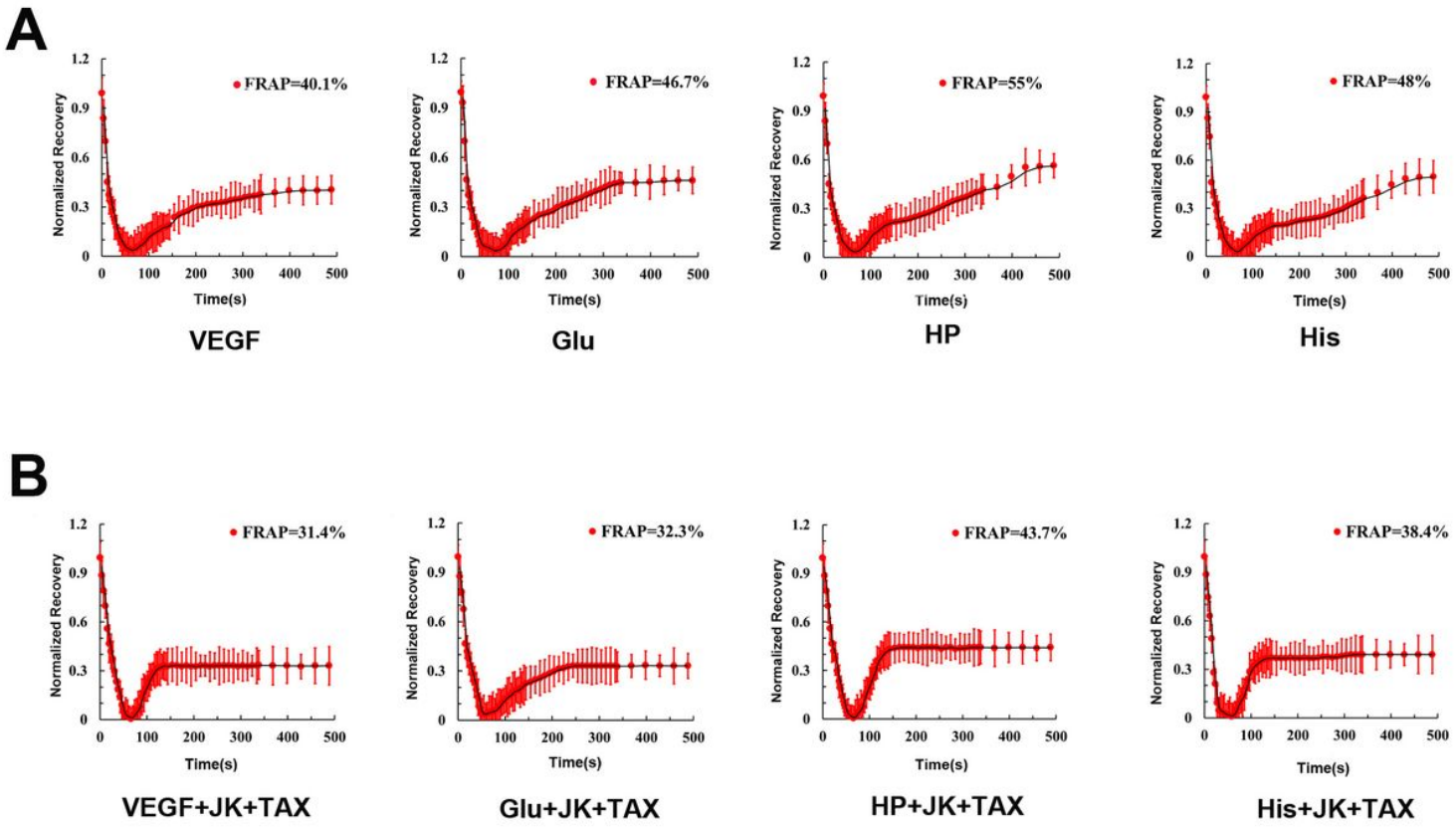

Figure 5

FRAP tests to examine occludin probe mobility on cytomembranes. A. Normalized FRAP recovery rate of occludin probe in HBMEC cells after treatment with VEGF, Glu, HP, and His. Normalized FRAP recovery rate of occludin probe in HBMEC cells in response to VEGF+JK+TAX, Glu+JK+TAX, HP+JK+TAX, and His+ JK+TAX treatment (n = 8).

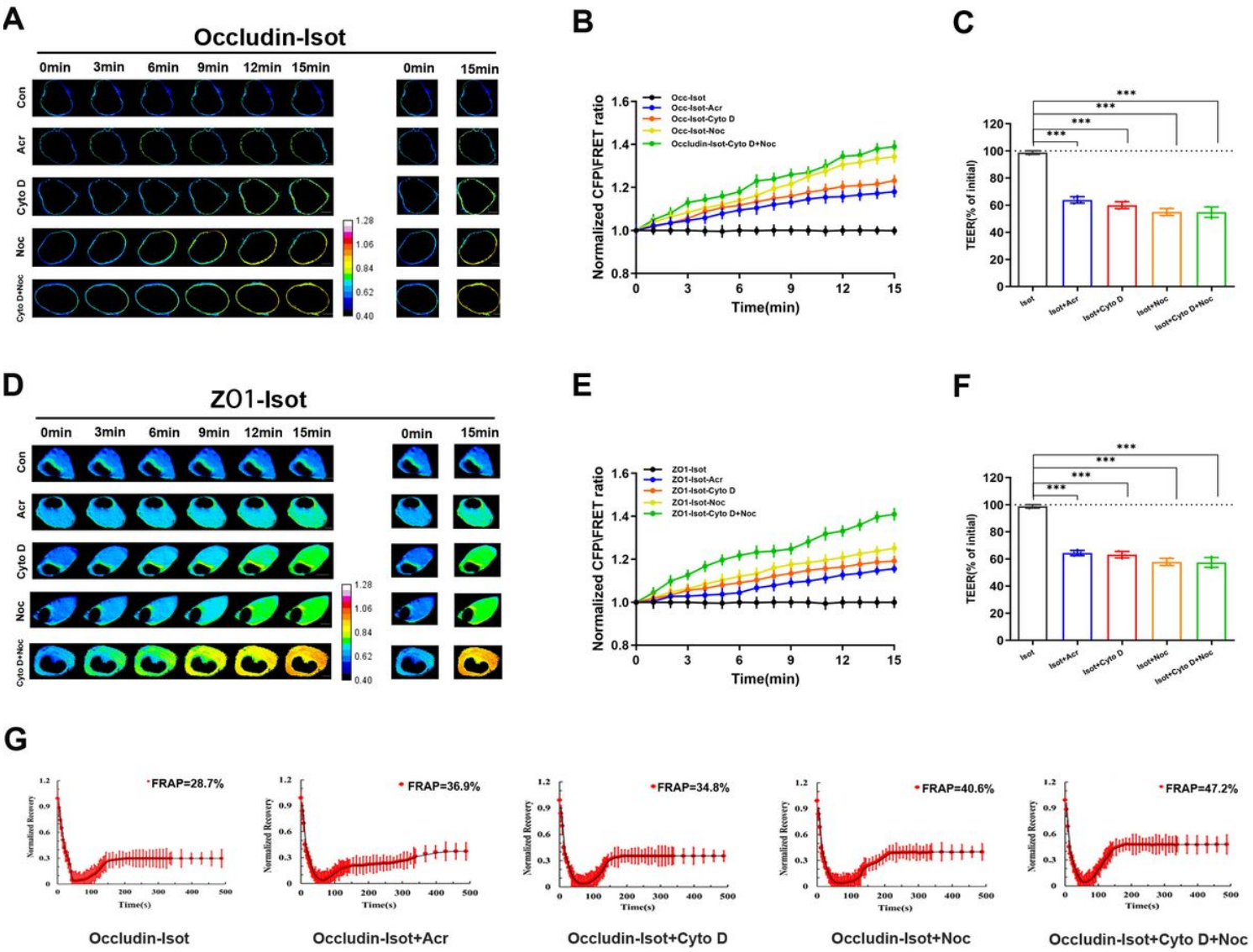

Figure 6

Changes in occludin/ZO1 tension and occludin mobility induced by cytoskeleton depolymerizers. A and D. Fluorescence images of (A) occludin and (D) ZO1 probe-transfected HBMEC cells treated with of Acr, Cyto D, Noc, or Cyto D+Noc over 15 min. B and E. Normalized CFP/FRET ratio of (B) occludin/ (E) ZO1 induced by the indicated agents in 15 min. Scale bar: 20 μm; the calibration bar was set from 0.40 to 1.28. C and F. Normalized TEER values in (C) Occludin and (F) ZO1 probe-transfected HBMEC cells in response to treatment with cytoskeleton depolymerizers. Data are shown as mean ± SD, n ≥ 5; *P < 0.05, **P < 0.01, ***P < 0.001. G. Normalized FRAP recovery rate of occludin probe in HBMEC cells treated with Acr, Cyto D, Noc, and Cyto D+Noc in isotonic conditions (n = 8).

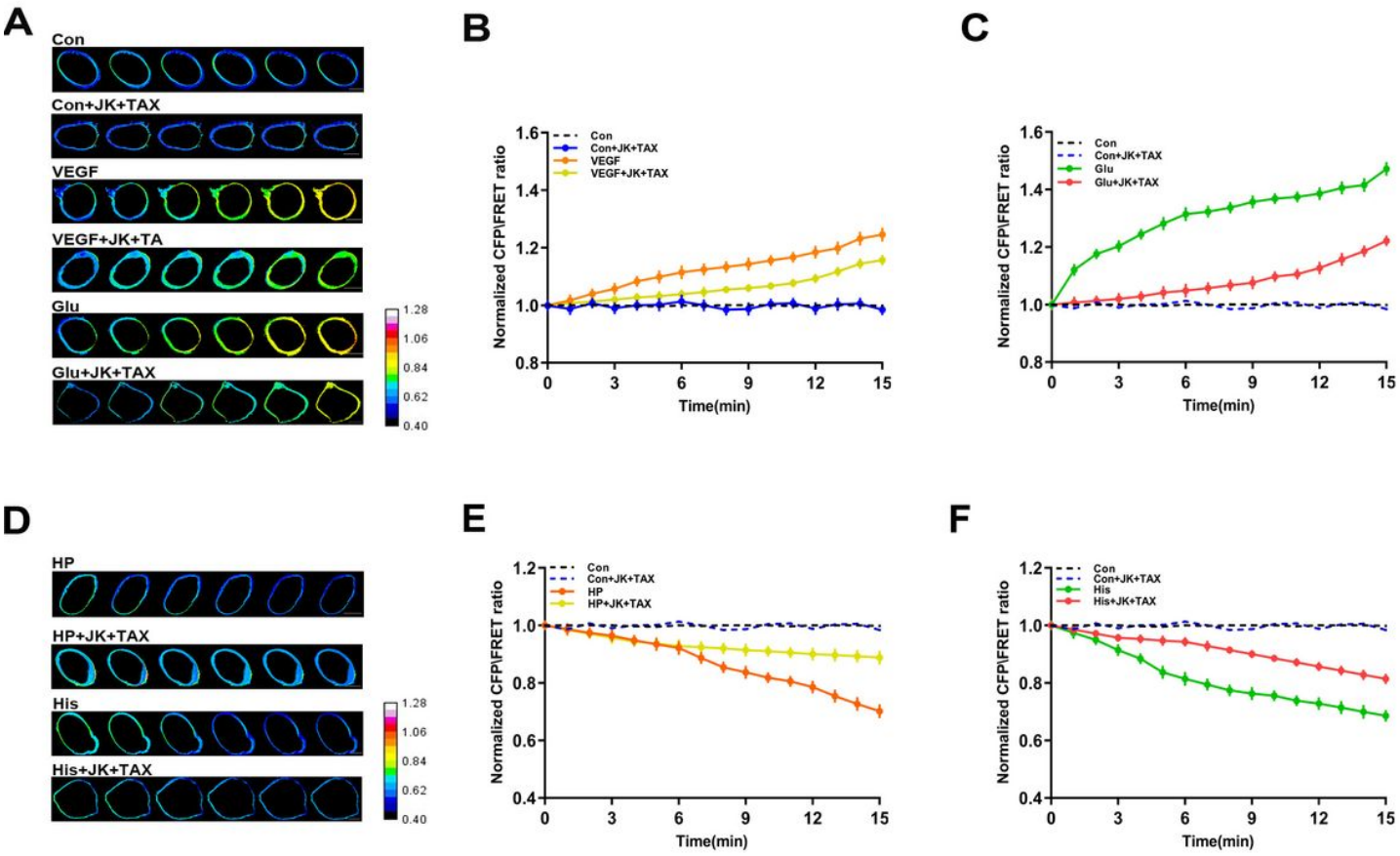

Figure 7

Effects of cytoskeleton stabilizers on occludin tension in HBMEC cells treated with BBB lesion agents. A. Fluorescence images of occludin probe- transfected HBMEC cells treated with con, con +JK+TAX, VEGF, VEGF+JK+TAX, Glu, or Glu+JK+TAX, for 15 min. B. Normalized CFP/FRET ratio in occludin probe-transfected HBMEC cells vs. time (15 min) after treatment with con, con+JK+TAX, VEGF, and VEGF+JK+TAX. C. Normalized CFP/FRET ratio in occludin probe-transfected HBMEC cells vs. time (15 min) after treatment with con, con+JK+TAX, Glu, and Glu+JK+TAX. D. Fluorescence images of occludin probe-transfected HBMEC cells treated with HP, HP+JK+TAX, His, and His +JK+TAX for 15 min. E. The normalized CFP/FRET ratio in occludin probe-transfected HBMEC cells vs. time (15 min) after treatment with con, con+JK+TAX, HP, and HP+JK+TAX. F. The normalized CFP/FRET ratio in occludin probe-transfected HBMEC cells vs. time (15 min) after treatment with con, con +JK+TAX, His, and His +JK+TAX. Data are presented as mean ± SEM; n ≥ 5; Scale bar: 20 μm; The calibration bar was set from 0.40 to 1.28.

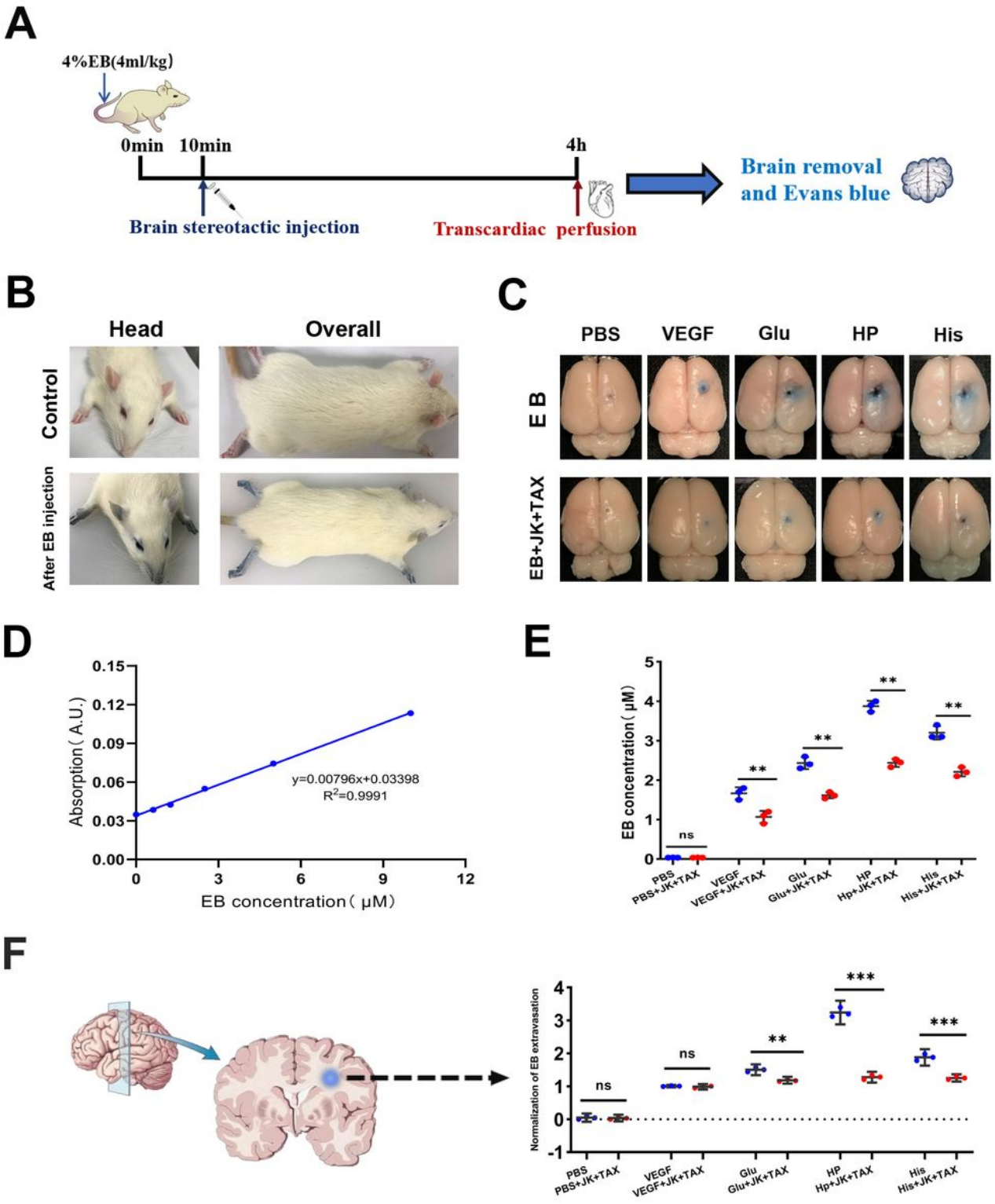

Figure 8

Roles of BBB lesion factors and cytoskeleton stabilizers in rat brain BBB permeability. A. Schematic representation of experimental design. B. Images of SD rat overall body 5 min after injection of EB. C. PBS, VEGF, Glu, HP, and His were stereotactically injected into rat brains after EB injection respectively. After 4 h of cardiac perfusion, brain images were taken to observe EB infiltration. D. EB standard curve. 0, 0.625, 1.25, 2.5, 5, and 10 μM EB solutions were made and OD value of absorption was measured. The

equation Y= 0.00796X + 0.03398, R2 = 0.9991 was used to calculate EB absorption. E. Quantification of EB exosmosis in rat brain. F. Quantitative analysis of EB extravasation in coronal slices of rat brain obtained in Fig. 7C. **P < 0.01, n=3.

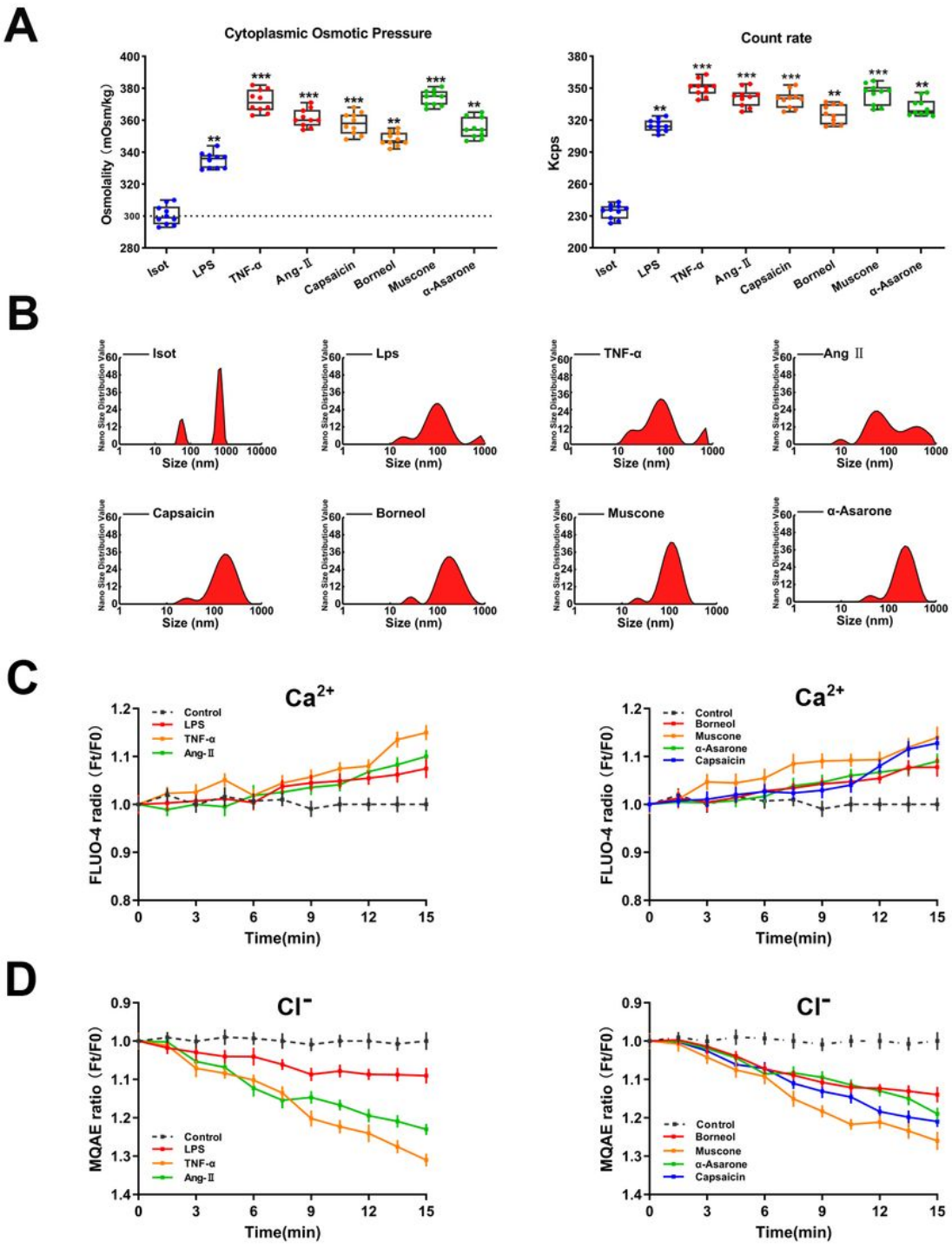

Figure 9

Roles of BBB lesion factors and cytoskeleton stabilizers in rat brain BBB permeability. A. Schematic representation of experimental design. B. Images of SD rat overall body 5 min after injection of EB. C.

PBS, VEGF, Glu, HP, and His were stereotactically injected into rat brains after EB injection respectively. After 4 h of cardiac perfusion, brain images were taken to observe EB infiltration. D. EB standard curve. 0, 0.625, 1.25, 2.5, 5, and 10 μM EB solutions were made and OD value of absorption was measured. The equation Y= 0.00796X + 0.03398, R2 = 0.9991 was used to calculate EB absorption. E. Quantification of EB exosmosis in rat brain. F. Quantitative analysis of EB extravasation in coronal slices of rat brain obtained in Fig. 7C. **P < 0.01, n=3.

Supplementary Files

This is a list of supplementary files associated with this preprint. Click to download.

- Fig.S1.jpg
- Fig.S2.jpg